Tensile ductility and necking of metallic glass

H. GUO[1], P. F. YAN[1], Y. B. WANG[1], J. TAN[1], Z. F. ZHANG[1], M. L. SUI[1]* AND E. MA[2]

[1]Shenyang National Laboratory for Materials Science, Institute of Metal Research, Chinese Academy of Sciences, Shenyang 110016, China

[2]Department of Materials Science and Engineering, The Johns Hopkins University, Baltimore, Maryland 21218, USA

*e-mail: mlsui@imr.ac.cn

Published online: 19 August 2007; doi:10.1038/nmat1984

Metallic glasses have a very high strength, hardness and elastic limit. However, they rarely show tensile ductility at room temperature and are considered quasi-brittle materials[1,2]. Although these amorphous metals are capable of shear flow, severe plastic instability sets in at the onset of plastic deformation, which seems to be exclusively localized in extremely narrow shear bands ~10 nm in thickness[3–13]. Using *in situ* tensile tests in a transmission electron microscope, we demonstrate radically different deformation behaviour for monolithic metallic-glass samples with dimensions of the order of 100 nm. Large tensile ductility in the range of 23–45% was observed, including significant uniform elongation and extensive necking or stable growth of the shear offset. This large plasticity in small-volume metallic-glass samples did not result from the branching/deflection of shear bands or nanocrystallization. These observations suggest that metallic glasses can plastically deform in a manner similar to their crystalline counterparts, via homogeneous and inhomogeneous flow without catastrophic failure. The sample-size effect discovered has implications for the application of metallic glasses in thin films and micro-devices, as well as for understanding the fundamental mechanical response of amorphous metals.

In sharp contrast to crystalline metals that have large tensile ductility including significant uniform elongation, monolithic metallic glasses show little or no macroscopically observable tensile strain at room temperature[1–13]. Under compressive loading with or without confinement, plasticity is often observable, but is always highly inhomogeneous. The strains are concentrated in narrow shear bands that are not only few in number but also tend to run wild to cause early failure. It is thus believed that the vast majority of the metallic-glass sample volume does not contribute to plastic deformation[1], and severe strain localization is the only deformation mode at temperatures well below the glass-transition temperature.

In the following, we demonstrate qualitatively different behaviour in small-volume metallic glasses. The behaviours common to ductile crystalline metals, including uniform elongation, necking and stable shear, can all happen when the sample dimensions of the metallic glasses are brought into the submicrometre to nanometre range. Hints for important changes in deformation modes have emerged recently in micrometre-sized samples[14–16] (Z.W. Shan *et al.*, unpublished). To observe the entire sequence of deformation stages in small samples, we carried out *in situ* tensile straining experiments in a transmission electron microscope (TEM) on several monolithic metallic-glass samples with dimensions in the 100 nm range.

The material studied was a typical bulk metallic glass, $Zr_{52.5}Cu_{17.9}Al_{10}Ni_{14.6}Ti_5$, prepared using copper-mould casting[10]. This alloy was studied previously in conventional mechanical tests[10]: the total plastic strain to failure was ~1% in compression and nearly zero in tension before fracture (the elastic strain was ~1.7%). A slice with dimensions of 45 μm (thickness) × 700 μm (width) × 3.3 mm (length) was cut from the bulk sample and glued to a brass substrate for *in situ* tension straining, as shown in Fig. 1a. Small test samples with a gauge section (the straight portion) of about 100 nm × 100 nm × 250 nm were fabricated near the centre of the upper edge of the slice (Fig. 1b), using the dual-focused-ion-beam (FIB) micromachining technique[17], as shown in the schematic diagrams in Fig. 1b–d. The final sample sets, as shown in scanning electron microscope (SEM) images (Fig. 1e,f) viewed from the angles in Fig. 1b,c respectively, were subjected to the *in situ* tensile straining experiments at a strain rate of about $\sim 5 \times 10^{-4}$ s^{-1}. The sample design, testing schemes and electron-beam-heating effects are discussed in the Methods section.

Figure 2 shows a series of video frames presenting the typical behaviour of sample I during the *in situ* tension experiment. Interestingly, measurements of the lengths of the gauge section (marked by dashed horizontal white lines) indicate that the sample uniformly elongated, up to a strain as high as 15% (Fig. 2b). This is the point when the first sign was observed for non-uniform deformation starting at a location slightly above the middle of the gauge section. One shear band was initiated, and the shear offset became obvious at the stage shown in Fig. 2c, where the total elongation reached 24%. This strain increment (from 15 to 24%) is partly a result of the slow growth of the shear offset, without the rapid fracture common in conventional metallic-glass test samples[8], and also of the preferential thinning of the material in the middle (Fig. 2c). This necked region (marked with an arrow in Fig. 2d) narrowed gradually and considerably, also contributing elongations without fracture, as shown in Fig. 2d,e. At the stage shown in Fig. 2e, the total tensile strain reached 45% (if we discount the strains non-uniformly concentrated in the thin neck in the middle, the rest of the gauge section experienced an elongation of 29%). We emphasize that the large strain here was not achieved through the formation of multiple shear bands[9–13,18–22].

Samples II and III both had some unevenness on the sample (side) surfaces after FIB cutting. These 'notches' in the virgin samples before testing served as stress concentrators and encouraged necking to start early during the *in situ* tensile straining experiments. Figure 3 shows a series of photos from the videotape, showing sample II at different straining stages. Necking was the dominant deformation mode (from Fig. 3b–e), starting from the pre-existing notch (marked with an arrow in Fig. 3a). The necked region had a very small volume, a complex stress state, and

© 2007 Nature Publishing Group

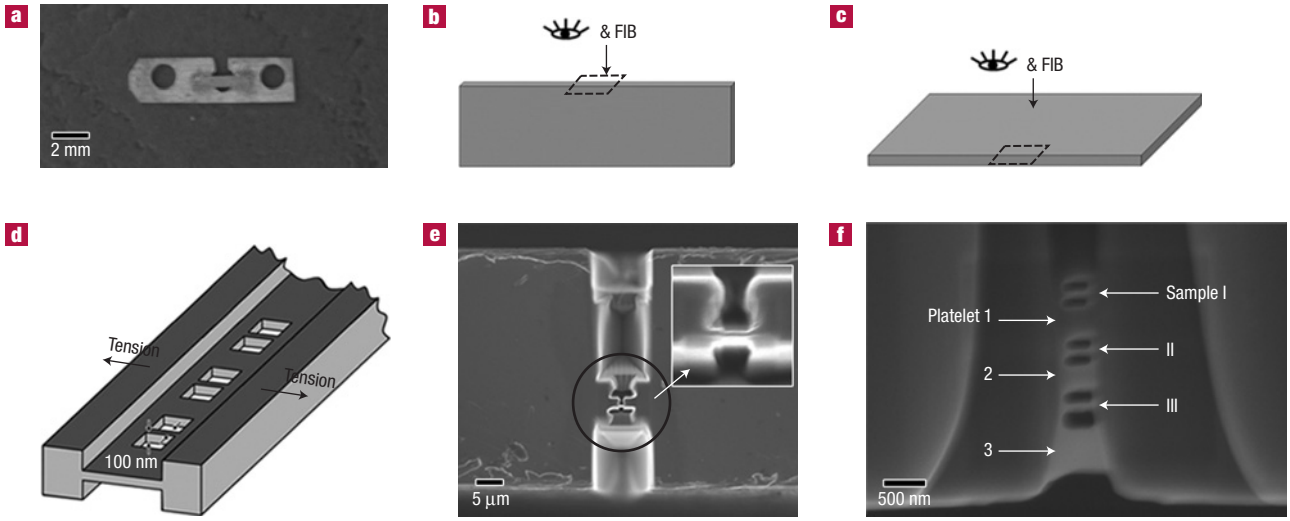

Figure 1 Small-volume metallic-glass samples for the *in situ* tensile straining experiment in the TEM. a, A slice of metallic glass glued to a brass substrate for *in situ* tension. **b**,**c**, Viewing directions for the first (**b**) and second (**c**) steps of FIB micromachining of the samples at the edge of the metallic-glass slice. **d**, A schematic diagram of the three submicrometre samples prepared using FIB. **e**, SEM image of the 100-nm-thick platelet fabricated, viewed from the angle in **b**. **f**, SEM image of the sample columns tested and their surrounding platelets (the dimensions are given in the text) separating the samples; the sample gauges had dimensions of 100 nm × 100 nm × 250 nm.

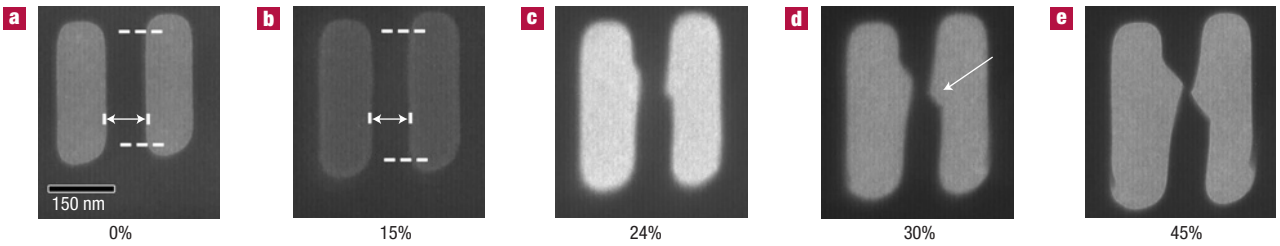

Figure 2 Sample I at various stages of tensile elongation during the *in situ* TEM experiment. The average strain rate was about 5×10^{-4} s^{-1}. The straight gauge section is marked with dashed white lines. **a**–**e**, This series of video frames demonstrates that the virgin sample before testing (**a**) was uniformly elongated to a strain of 15% (**b**), where non-uniform deformation began; one major shear was initiated, and the shear offset grew with further straining together with significant elongation in the necked region indicated by the white arrow (**c**–**e**). The tensile strain for **e** reached 45%.

the aspect ratio was low resulting in confinement[12,13], such that continued 45° shear was not favoured[23]. In fact, throughout the test shear did not localize on one dominant plane. The necked region enlarged and spread out gradually, and the extensive necking led to an elongation to failure of 23% in Fig. 3e after recovering the elastic strain. It is well known that gradual necking only occurs in ductile metallic materials, and the area reduction ratio, $\Psi = (A_0 - A)/A_0$, where A is the area after necking (see Fig. 4) and A_0 is the original area, is a measure of the ductility. The eventual Ψ at fracture for sample II is as high as ~80%. Such extraordinary ductility has never been observed in metallic glasses; some signs of necking were occasionally observed only when large volume fractions of ductile crystalline dendrites were added into a glass to form metallic-glass composites[9].

Sample III behaved in the same manner as sample II. In addition, see above for sample I for the large post-uniform deformation. To further check the reproducibility of the results, a separate batch consisting of two further samples was made and they both fractured with obvious necking. This suggests that the necking behaviour reported above is common for such small-volume bulk metallic glasses under tensile loading. The easy occurrence of the necking instability in tension is expected for a material such as monolithic metallic glass that does not possess an obvious mechanism for strain hardening[1,23]. To reproduce the major shear reported for sample I in Fig. 2, we should suppress surface undulations (Fig. 3) that could accelerate early necking. This was difficult for the 100 nm samples using our current FIB cutting procedures. However, such behaviour should be easily captured in compression tests, in which the sample is not subject to the necking instability. Indeed, *in situ* TEM videos of several samples of a similar Zr–Cu–Al metallic glass in nanocompression tests showed nearly homogeneous deformation followed by slow, stable growth of the shear offset on a shear band after it is initiated (Z.W. Shan *et al.*, unpublished).

The wider platelets surrounding samples I to III also offered the opportunity to observe the behaviour in Fig. 2. This is because necking is known to start at larger critical strains for the thin-plate geometry, and here the edge undulations also have smaller effects because they are minor compared with the platelet width. Indeed, homogeneous deformation also occurred in the three platelets up to an elongation of about 14%, followed by localized shear in various directions. These platelets also have dimensions in the

© 2007 Nature Publishing Group

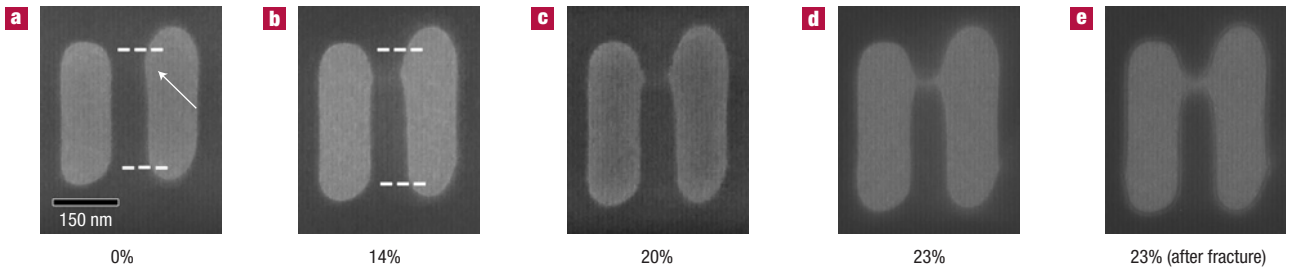

Figure 3 The necking process in sample II observed during the *in situ* tensile testing in the TEM. a–e, The 'notches' on the surfaces in the virgin sample (indicated by the white arrow in **a**) encouraged necking to start early, developing extensively and gradually (**b–e**). The strain to failure at **e** reached 23%, and the area reduction ratio at fracture is as high as ~80% (also see the close-up views in Fig. 4).

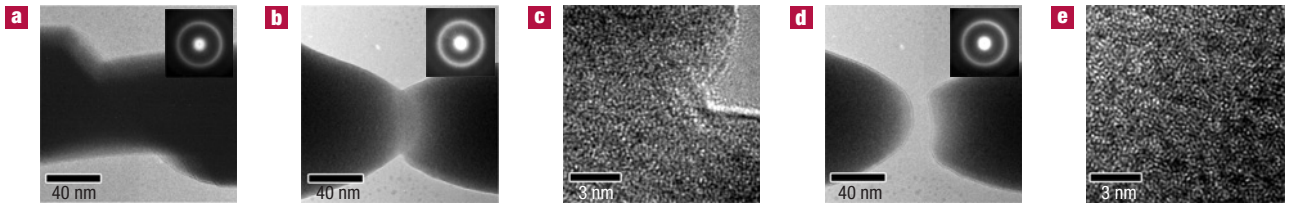

Figure 4 TEM bright-field images and corresponding electron diffraction patterns (insets) of the *in situ* tested samples at various stages of straining. a, Sample I at an elongation of about 24%. **b**, The necked region in sample II at an elongation of about 20%, before fracture. **c**, HRTEM image of the region shown in **b**. **d**, The eventually fractured region in sample II. **e**, The HRTEM image corresponding to **d**. All of the images and electron diffraction patterns confirm that no crystallization occurred throughout the experiment.

submicrometre regime, such that the localized deformation was also stable. In fact, the wider platelets continued to deform without reaching final failure, after the three samples fractured one after another. Apparently the larger volumes of the platelets provided more room for accommodating the damage (localized strains).

Figure 4a shows a TEM bright-field image of sample I, taken at a tensile strain of about 24%. There is no change of contrast, which is consistent with the diffraction pattern in the inset indicating no induced crystallization even in the heavily deformed region. Figure 4b shows the TEM bright-field image of sample II after pronounced necking but before fracture. The inset electron diffraction pattern again shows that no crystallization occurred, which is further confirmed by the high-resolution TEM (HRTEM) image in Fig. 4c. Even after fracture, both the electron diffraction pattern (inset in Fig. 4d) and the HRTEM image in Fig. 4e indicate that crystallization was never induced in this heavily strained necked region. This is also true for other necked and fractured samples, as confirmed with post-fracture diffraction and dark-field examinations. These observations are consistent with a low deformation temperature in our test samples. The plasticity here comes entirely from the flow of the monolithic glass, very different from the deflection and branching of shear bands due to surrounding nanocrystals as suggested previously for the compressive plasticity observed in some metallic glasses[8,11,24].

Homogeneous deformation of metallic glasses is known to occur only when the test temperature is elevated to above[1], or at least close to, the glass-transition temperature ($T_g = 675$ K for our glass). In that case large ductility is achieved owing to viscous flow, which commands a high strain-rate sensitivity leading to superplastic-like behaviour without necking. In the low-temperature regime, homogeneous deformation with uniform elongation, or non-uniform deformation via extensive necking, was predicted for extremely small wires in molecular dynamics simulations, which were only able to handle a diameter of 13.6 nm (ref. 23). Our findings indicate remarkable sample-size effects: the small volume delays catastrophic localization and increases failure resistance, leading to large tensile elongations.

Let us examine these effects from several angles. First, the sample dimension is now well below the normal range of the shear-band spacing (typically micrometres) observed in samples after conventional tests[1,11,25–27]. The small sample volume is less likely to contain flaws, or (pre-damaged) fertile sites, for the initiation of a severely localized shear band. There is also limited room for a major instability (a particular Fourier component) to grow to dominance out of the fluctuating shear events ongoing throughout the sample[27]. This reduces the probability of forming a predominant instability that pre-empts homogeneous deformation. Without severe shear banding that concentrates all of the strains exclusively on one plane, throughout the sample the individual shear-transformation zones (or their groups)[28] and the local redistribution of free volume[29] have the opportunity to mediate multiple atomic-level shear events. These 'dislocation-like' shear events, happening all over the small volume, render elongations that seem homogeneous over a range of strains (Fig. 2). The results of compression tests of microscale or nanoscale metallic-glass samples[14–16] (Z.W. Shan *et al.*, unpublished) also support this observation. Note that the shear transformations, being thermally activated and stress-assisted processes, always have a finite chance to contribute to deformation at sufficiently high stresses[1].

Second, even after localization begins, for example, with the presence of a minor notch that led to necking (Fig. 3) or after a major shear that eventually sets in (Fig. 2), in small-volume metallic glasses failure does not immediately ensue. This can be rationalized from several perspectives. The plastic zone size at the

© 2007 Nature Publishing Group

tip of an incipient crack[30], d, is determined by the squared ratio of the fracture toughness to the yield strength, and is much larger than 1 μm for Zr-based metallic glasses[30] and hence much larger than our sample size. As a result, brittle failure due to catastrophic crack propagation is disfavoured[16,30]. This could also be argued from the driving-force perspective. The elastic strain energy stored in the volume scales with L^3, where L is the sample dimension. The surface energy the cracking has to overcome scales with L^2. As the sample volume is reduced, the former decreases much faster than the latter, such that in nanoscale volumes brittle fracture is difficult. We can also assume that there is a critical length, typically larger than several micrometres for metallic glasses[1,25], for the shear offset to turn into a runaway crack. Such a critical length is not reachable in nanosized samples. An instability, for example in the form of shear localization or a neck, is therefore under control and propagates/expands without inducing immediate catastrophic fracture, as shown in Figs 2 and 3.

Another way to look at the sample-size effect is to consider that for a shear band to be fully developed and enter a mature stage, its nucleus would need a size of the order of 50−500 nm (refs 1,31). In other words, for an embryonic shear band to go critical, it requires a running distance for it to accelerate to its full propagation speed. Small samples such as ours do not provide a runway sufficiently long for this to happen. As a result, a shear localization in our case is in the incipient stage of a shear band and does not become one that is as excessively hot and dangerous as those in large samples[31]. The growth of the shear step is therefore slow and progressive (also seen in compression tests of nanoscale metallic-glass samples (Z.W. Shan *et al.*, unpublished)). Meanwhile, the atomic-level flow events (as discussed above) nearby but elsewhere are given the chance to participate in the accommodation of the strain (rate) imposed, contributing to elongation. A neck may get to develop and the necking progresses gradually and extensively before fracture (see Figs 2 and 3).

In summary, large tensile strains have been demonstrated, via both homogeneous and inhomogeneous deformation, for monolithic metallic glasses. This happens in small-volume specimens, owing to sample-size effects suppressing catastrophic localization and failure. Homogeneous deformation followed by necking tends to become the dominant mode when the deforming sample volume decreases to approach that of a typical shear band[23,32]. The *in situ* TEM experiments also indicate that large plasticity in metallic glasses does not necessarily require the multiplication of shear bands or the presence of (nano)crystals. Monolithic metallic glasses can be intrinsically malleable as well as truly ductile in tension.

METHODS

The first step in making the small samples was to prepare, using FIB, a thin plate with dimensions of 100 nm (thickness) × 500 nm (width) × 10 μm (length). Figure 1e shows an SEM view from the top (Fig. 1b) of the thin plate fabricated. Pairs of slits (∼150 nm × ∼300 nm) were then cut into the plate. Between two slits machined next to each other the remaining material was only 100 nm wide, giving the sample a gauge section (the straight portion) of about 100 nm × 100 nm × ∼250 nm. An SEM micrograph of the final sample set (hereafter referred to as sample I, II, and III) is shown in Fig. 1f, viewed from the angle in Fig. 1c. The metallic-glass plate regions left would deform together with the samples on loading. They will be referred to as platelet 1, 2 and 3 (see Fig. 1f), with dimensions of 100 nm × ∼500 nm × ∼300 nm. To reduce the possible damage to the sample surfaces caused by the Ga ions, the desired dimensions were reached with gradually reduced FIB beam currents, and the current density used for the final trim was about 50 pA. The energy-dispersive X-ray spectroscopy results showed that the Ga was incorporated in the sample surface at a low concentration of <1%, and TEM examination confirmed that FIB processing did not affect the amorphous nature of the samples.

In situ tensile straining experiments were carried out at room temperature using an FEI Tecnai F30 TEM operating at 300 kV with a Gatan Model 654 single-tilt straining holder. The deformation behaviour, sample morphologies and the final fracture were recorded using digital videotaping in the microscope. The strains were applied by applying intermittent displacement pulses manually through a trigger switch that activated a motor in the straining holder. All of the samples and platelets were being pulled at the same time, but our design of multiple samples and platelets at various locations and with different sizes made it possible for the deformation events (for example, necking, fracture and so on) not to start (and finish) all at the same time.

The entire deformation process for each sample took about several minutes, but our e-beam illumination and videotaping was carried out for about one minute at a time, rather than continuously for each sample. In other words, the beam was alternately focused on different gauge sections and platelets while the others continued to deform without being observed or exposed to the beam. For a given sample, its deformation mode could not be controlled by beam effects, because much of its elongation occurred when the e-beam was moved to observe other samples one after another. The beam-heating effects should also be small because the temperature rise was estimated to be insignificant as our specimen was part of a large metal piece (Fig. 1) with a good thermal conductivity[33] ($20\ W\ mK^{-1}$). We stopped straining the sample several times to quickly take bright-field TEM images, diffraction patterns and HRTEM images, without unloading the stress.

The strain rate was estimated to be typically about $\sim 5 \times 10^{-4}\ s^{-1}$, by using the strain difference in the gauge length (between the start and the end of a continuous video segment) divided by the time elapsed in the video clip. This rate is of a similar order of magnitude to that used for conventional testing of large metallic-glass samples. Such a slow rate was made possible by the specimen design scheme, that is, multiple samples with controlled geometry and protective platelets in Fig. 1f and the lower-strength buffer brass substrate shown in Fig. 1a. This assembly removed much of the imposed strain such that the deformation in the local FIB-treated sample area was moderate. It should be mentioned that the FIB-smoothed sample edges (∼100 nm) are relatively thick and rounded, reducing the unwanted stress concentration. In comparison, the perforated locations obtained by ion-milling thinning in previous *in situ* TEM tensile studies of metallic glasses[34] had very thin edges, uncontrollable geometries and stress states, and the highly concentrated forces usually caused immediate and rapid cracking.

Received 11 June 2007; accepted 18 July 2007; published 19 August 2007.

References

1. Schuh, C. A., Hufnagel, T. C. & Ramamurty, U. Mechanical behavior of amorphous alloys. *Acta Mater.* **55**, 4067–4109 (2007).
2. Sergueeva, A. V., Mara, N. A., Branagan, D. J. & Mukherjee, A. K. Strain rate effect on metallic glass ductility. *Scr. Mater.* **50**, 1303–1307 (2004).
3. Johnson, W. L. Bulk glass-forming metallic alloys: Science and technology. *Mater. Res. Soc. Bull.* **24**, 42–56 (1999).
4. Pampillo, C. A. & Chen, H. S. Compressive plastic deformation of a bulk metallic glass. *Mater. Sci. Eng.* **13**, 181–188 (1974).
5. Davis, L. A. & Yeow, Y. T. Flow and fracture of a Ni–Fe metallic glass. *J. Mater. Sci.* **15**, 230–236 (1980).
6. Liu, C. T. *et al.* Test environments and mechanical properties of Zr-base bulk amorphous alloys. *Metall. Mater. Trans. A* **29**, 1811–1820 (1998).
7. Lewandowski, J. J. & Lowhaphandu, P. Effects of hydrostatic pressure on the flow and fracture of a bulk amorphous metal. *Phil. Mag. A* **82**, 3427–3441 (2002).
8. Yavari, A. R., Lewandowski, J. J. & Eckert, J. Mechanical properties of bulk metallic glasses. *Mater. Res. Soc. Bull.* (August 2007).
9. Hays, C. C., Kim, C. P. & Johnson, W. L. Microstructure controlled shear band pattern formation and enhanced plasticity of bulk metallic glasses containing in situ formed ductile phase dendrite dispersions. *Phys. Rev. Lett.* **84**, 2901–2904 (2000).
10. Zhang, Z. F., Eckert, J. & Schultz, L. Fatigue and fracture behavior of bulk metallic glass. *Metall. Mater. Trans. A* **35**, 3489–3498 (2004).
11. Inoue, A., Zhang, W., Tsurui, T., Yavari, A. R. & Greer, A. L. Unusual room-temperature compressive plasticity in nanocrystal-toughened bulk copper-zirconium glass. *Phil. Mag. Lett.* **85**, 221–229 (2005).
12. Zhang, Z. F., Zhang, H., Pan, X. F., Das, J. & Eckert, J. Effect of aspect ratio on the compressive deformation and fracture behaviour of Zr-based bulk metallic glass. *Phil. Mag. Lett.* **85**, 513–524 (2005).
13. Bei, H., Xie, S. & George, E. P. Softening caused by profuse shear banding in a bulk metallic glass. *Phys. Rev. Lett.* **96**, 105503 (2006).
14. Volkert, C. A., Cordero, N., Lilleodden, E. T., Donohue, A. & Spaepen, F. in *Size Effects in the Deformation of Materials—Experiments and Modeling* (eds Lilleodden, E., Besser, P., Levine, L. & Needleman, A.) (Mater. Res. Soc. Symp. Proc., Vol. 976E, Materials Research Society, Warrendale, 2007).
15. Spaepen, F. in *Processing-Structure-Mechanical Property Relations in Composite Materials* (eds Thilly, L., Moody, N. R., Misra, A., Anderson, P. M. & Kumar, M.) (Mater. Res. Soc. Symp. Proc., Vol. 977E, Materials Research Society, Warrendale, 2007).
16. Zheng, Q., Cheng, S., Strader, J. H., Ma, E. & Xu, J. Critical size and strength of the best bulk metallic glass former in the Mg–Cu–Gd ternary system. *Scr. Metall.* **56**, 161–164 (2007).
17. Uchic, M. D., Dimiduk, D. M., Florando, J. N. & Nix, W. D. Sample dimensions influence strength and crystal plasticity. *Science* **305**, 986–989 (2004).

© 2007 Nature Publishing Group

18. Schroers, J. & Johnson, W. L. Ductile bulk metallic glass. *Phys. Rev. Lett.* **93**, 255506 (2004).
19. Das, J. *et al.* "Work-hardenable" ductile bulk metallic glass. *Phys. Rev. Lett.* **94**, 205501 (2005).
20. Liu, Y. H. *et al.* Super plastic bulk metallic glasses at room temperature. *Science* **315**, 1385–1388 (2007).
21. Zhang, Y., Wang, W. H. & Greer, A. L. Making metallic glasses plastic by control of residual stress. *Nature Mater.* **5**, 857–860 (2006).
22. Bae, D. H., Lee, S. W., Kwon, J. W., Yi, S. & Park, J. S. Deformation behavior of Zr–Al–Cu–Ni–Sn metallic glasses. *J. Mater. Res.* **21**, 1305 (2006).
23. Li, Q. & Li, M. Molecular dynamics simulation of intrinsic and extrinsic mechanical properties of amorphous metals. *Intermetallics* **14**, 1005–1010 (2006).
24. Chen, M., Inoue, A., Zhang, W. & Sakurai, T. Extraordinary plasticity of ductile bulk metallic glasses. *Phys. Rev. Lett.* **96**, 245502 (2006).
25. Wu, F. F. *et al.* Multiplication of shear bands and ductility of metallic glass. *Appl. Phys. Lett.* **90**, 191909 (2007).
26. Conner, R. D., Johnson, W. L., Paton, N. E. & Nix, W. D. Shear bands and cracking of metallic glass plates in bending. *J. Appl. Phys.* **94**, 904–901 (2003).
27. Wright, T. W. & Ockendon, H. A scaling law for the effect of inertia on the formation of adiabatic shear bands. *Int. J. Plasticity* **12**, 927–934 (1996).
28. Argon, A. S. & Kou, H. Y. Plastic flow in a disordered bubble raft (an analog of a metallic glass). *Mater. Sci. Eng.* **39**, 101–109 (1979).
29. Spaepen, F. A microscopic mechanism for steady state in homogeneous flow in metallic glasses. *Acta Metall.* **25**, 407–415 (1977).
30. Ashby, M. F. & Greer, A. L. Metallic glasses as structural materials. *Scr. Mater.* **54**, 321–326 (2006).
31. Schuh, C. A., Lund, A. C. & Nieh, T. G. New regime of homogeneous flow in the deformation map of metallic glasses: Elevated temperature nanoindentation experiments and mechanistic modeling. *Acta Mater.* **52**, 5879–5891 (2004).
32. Wang, Y. M., Li, J., Hamza, A. V. & Barbee, T. W. Jr. Ductile crystalline-amorphous nanolaminates. *Proc. Natl Acad. Sci.* **104**, 11155–11160 (2007).
33. Hobbs, L. W. *Introduction to Analytical Electron Microscopy* Ch. 17 (Plenum, New York, 1979).
34. Hajlaoui, K. *et al.* Shear delocalization and crack blunting of a metallic glass containing nanoparticles: In-situ deformation in TEM analysis. *Scr. Mater.* **54**, 1829–1834 (2006).

Acknowledgements

Financial support from the National Nature Science Foundation of China (Grant Nos 50125103, 50671104 and 50625103) and the 'Hundred of Talents Project' of the Chinese Academy of Science (CAS) are gratefully acknowledged. The authors were also part of the MANS research team, supported in part by CAS.
Correspondence and requests for materials should be addressed to M.L.S.

Competing financial interests

The authors declare no competing financial interests.

Reprints and permission information is available online at http://npg.nature.com/reprintsandpermissions/

© 2007 Nature Publishing Group